Scientia Iranica A (2020) 27(5), 2264–2282

SCIENTIA IRANICA

Sharif University of Technology
Scientia Iranica
Transactions A: Civil Engineering
http://scientiairanica.sharif.edu

Seismic evaluation of special steel moment frames subjected to near-field earthquakes with forward directivity by considering soil-structure interaction effects

S. Shahbazi[a], M. Khatibinia[b], I. Mansouri[c,d], and J.W. Hu[e,f,*]

a. *TAAT Investment Group, Tehran, P.O. Box 18717-13553, Iran.*
b. *Department of Civil Engineering, University of Birjand, Birjand, Iran.*
c. *Department of Civil Engineering, Birjand University of Technology, Birjand, P.O. Box 97175-569, Iran.*
d. *Institute of Research and Development, Duy Tan University, Da Nang 550000, Vietnam.*
e. *Department of Civil and Environmental Engineering, Incheon National University, 12-1 Songdo-dong, Yeonsu-gu, Incheon 22012, South Korea.*
f. *Incheon Disaster Prevention Research Center, Incheon National University, 12-1 Songdo-dong, Yeonsu-gu, Incheon 406-840, South Korea.*

Received 10 January 2018; received in revised form 24 August 2018; accepted 3 December 2018

KEYWORDS
Soil-structure interaction;
Near-field;
Forward directivity;
Special moment frame;
Seismic response.

Abstract. Assuming that the bottom soil of the foundation is rigid and flexibility effect is ignored, the seismic response of a structure is influenced by its dynamic properties and soil flexibility does not affect the mentioned response. Hence, considering the analytical results only based on the fixed base buildings can result in an unsafe structure design. Therefore, near-field earthquakes produce many seismic needs to force the structure to dissipate this input energy with relatively large displacements. Accordingly, the primary objective of the present paper is to determine the seismic response of the 3-, 5-, and 8-story steel buildings with the special moment frame system, considering the soil-structure interaction and panel zone modeling. To this end, selected records of the near- and far-field earthquakes were used to facilitate the nonlinear time history analysis of the structures, whose responses to earthquakes were compared in both of the mentioned states. The results showed that the average drift of all three structures under the effect of near-field earthquakes was two times larger than the drift of the structures under the effect of the far-field earthquakes.

1. Introduction

A notable number of seismic researches have only focused on the responding ability and lateral resistance ductility of structures against earthquake and, therefore, effects of bottom soil of a structure on its seismic response have been left unexplored.

Usually, to carry out structural analysis, the effects of the Soil-Structure Interaction (SSI) are ignored and the seismic response of a structure is measured with the assumption of rigid foundation. However, during and after an earthquake, the bottom soil of a structure undergoes some transformation from the structure's foundation; hence, the dynamic response of the structure is affected by the altered behavior of the bottom soil.

*. *Corresponding author. Tel.: +82 328358463; Fax: +82 328350775*
E-mail addresses: shahrokh.shahbazi25@yahoo.com (S. Shahbazi); m.khatibinia@birjand.ac.ir (M. Khatibinia); mansouri@birjandut.ac.ir (I. Mansouri); jongp24@inu.ac.kr (J.W. Hu)

doi: 10.24200/sci.2018.50241.1594

The seismic response of a structure depends on different factors such as site type, specifications of ground motion, bottom and surrounding soil of a structure, and dynamic features of a structure [1]. In the case of structures constructed on the bedrock or soils with high hardness, the foundation movement is exactly similar to the ground motion built on the soil level. This movement is known as a free field movement; however, in soft soils, this definition is different for the aforementioned system (a structure constructed on the bedrock).

The difference of the definition results from the reflection and dispersion of seismic waves released into the soil of the structure foundation and the radiation energy originating from the vibration of the structure. Due to these effects, transformation (particle displacement, velocity, and acceleration) and ground motion in the bottom soil of a structure and in the free field movement are different [2,3]. Hence, in terms of amplitude and frequency content, the dynamic response of a structure constructed on the soft soil layers is fundamentally different from that of a similar structure constructed on the bedrock or the soils with high hardness [4,5].

The interaction effect on the nonlinear behavior of the structures was evaluated by Rodrigues and Montes [6]. Having considered the soil conditions of the area, the authors concluded that the desired effects of the SSI could be achieved using a period modification of the structure. Furthermore, Behnamfar et al. [7] studied the effects of uplift and SSI on the nonlinear seismic behavior of structures. The effect of spatially varying ground motions and SSI on the responses of the multiple-frame bridges was also evaluated in [8]. In addition, Zheng et al. [9] proposed a nonlinear two-degree-of-freedom model to study seismic responses of a bridge-foundation system. Likewise, Fatahi and Tabatabaiefar [10] studied the effects of plasticity index changes on the seismic response of mid-rise frames placed on soft soil deposits. In an experimental study, Hosseinzadeh [11] examined the effects of the SSI on the proposed experimental model.

The effect of the SSI on the nonlinear response of the high-rise structures was also examined by Nateghi-A and Rezaei-Tabrizi [12]. To this end, they carried out the nonlinear dynamic analysis and applied the finite element method and observed that, in cases where the dynamic frequency time of soil layers has a long distance from the structure period, the interaction of the adjacent structures revealed a reduction in nonlinear response and structural damage. In another study, Liao et al. [13] used viscose elements to model the area around soil and considered nonlinear properties of soil in their model. Furthermore, the results of Sáez et al. [14] showed that the nonlinear effect of the SSI significantly changed the seismic response of a structure, as compared to the fixed-base condition. Furthermore, El Ganainy and El Naggar [15] evaluated the steel moment frame building and concluded that the seismic response of the structures including shear strength of stories, moment of stories, and deformation of structural elements could be affected. According to these findings, the role of the SSI in soft soils has been reportedly much more important than that in hard soils.

Likewise, in order to determine the seismic response of a reinforced concrete moment frame building, Tabatabaiefar and Massumi [16] examined four types of structures subjected to three soil types with and without SSI . The authors introduced a coefficient and applied it to maximum lateral displacements of elastic structures with a fixed base. Then, they determined the maximum lateral displacement of an equal structure-soil interaction system. Furthermore, Gharehbaghi et al. [17] employed a direct method to investigate the effects of the SSI on the seismic behavior of the frame by which seismic energy demand in reinforced concrete moment frames was studied.

In addition, Khatibinia et al. compared 6- and 9-story buildings, through which the optimum design of concrete structures was evaluated using SSI effects [18,19].

In their study of near-field earthquakes, Masaeli et al. [20] investigated the negative and positive aspects of SSI. Mitropoulou et al. [21] applied the 3D reinforced concrete and steel building structures to study the SSI effect on the structural fragility assessment of such structures. Based on a comparison of the outcomes of fragility analysis, it was observed that, in the case of the low- and mid-rise buildings, the structural performance was not significantly affected by the foundation system. However, it was observed that the foundation system considerably contributed to the overall structural performance of high-rise structures. Besides the SSI, another relevant issue is the destructive effects of near-field earthquakes as compared to far-field ones. In fact, near-field earthquake characteristics cause the energy to release [3,22], which, due to faulting, appears at the beginning of earthquake record like a long-period pulse. Hence, this process improves the acceleration response at low frequencies [23].

Furthermore, Liu et al. [24] proposed the relationship between the earthquake record parameters and the reinforcement loads and residual facing displacement under near-field records. To simplify the direct method for the SSI analysis, Syyadpour et al. [25] proposed a procedure called the near-field method. The seismic behavior of nuclear power plants subjected to near-field ground motions considering the effect of SSI was studied by Abell et al. [26]. A numerical method for nonlinear SSI in a layered poroelastic half-space using the Drucker-Prager plastic model was introduced by Lee [27]. The SSI analysis of reinforced concrete

moment-resisting frames subjected to near-field records was carried out by Emami and Halabian [28]. Furthermore, Khoshnoudian et al. [29] applied the SSI analysis to the structures equipped with Tuned Mass Damper (TMD) with near-field ground motions. The authors concluded that TMD became less effective in reducing the response of frames to base excitation. Bybordiani and Arıcı [30] evaluated the effect of the ground motion scaling method on the dynamic analysis of concrete gravity dams considering the SSI effects and near-field records. The findings of Cheng et al. [31] on sliding base-isolated liquid storages under near-field earthquakes demonstrated that SSI amplified liquid sloshing height; however, the acceleration of the structure was found to be reduced due to SSI. An extensive parametric study was carried out by Behnamfar and Sayyadpour [32] using an elastoplastic constitutive relation for the soil under near-field ground motions. Johari et al. proposed a formulation to predict design parameters of retaining wall considering SSI [33]. The effect of toe condition and soil relative density on the soil-pile interaction was investigated by Azizkandi et al. [34].

The effects of forward directivity represent the reason why the recorded movements near the active faults have different properties opposing the ordinary movements recorded at a long distance of the fault. These motions are characterized by various properties including long-period pulses existing in the acceleration time history, velocity and displacement, the ratio of maximum velocity to maximum acceleration, and seismograph's high-frequency content and short-term durability of vertical components on the fault.

The present study evaluates the seismic behavior of steel structures with a Special Moment Frame (SMF) system. This structural system was selected in accordance with the engineers' expectation of high plasticity and attention to the nature of the near-field earthquakes with progressive direction taking. In this type of records, the structure does not have sufficient time to employ all its plasticity against the pulse-like behavior of these records due to the pulse-like behavior of the earthquake. To put it differently, these records act as a strong pulse in a long period on the structure while the authors have high expectations of the SMF system.

The properties mentioned above have different effects on structures. Furthermore, whip-like motion can be created from energy accumulation in the short-term period. In recent years, many studies have compared the destructive effects of near-field earthquakes and far-field ones. For instance, Tajammolian et al. [35] and Yin et al. [36] investigated the seismic behavior of steel structures equipped with triple concave friction pendulum under near-field earthquakes.

In sum, most previous studies have dealt with the evaluation of the seismic behavior of structures under the effect of far- and near-field earthquakes. However, none of these studies has thoroughly investigated the simultaneous effects of both earthquake directivity and SSI. Considering that high damping energy is expected of a SMF system, the present paper evaluates the seismic response of 3-, 5-, and 8-story special steel moment frames under near-field earthquakes with forward directivity and far-field earthquakes. To model these frames, the effects of panel zone and SSI have been considered in analyzing the seismic response of the structure.

2. Numerical modeling

2.1. Selecting the prototype building model

In the present study, 3-, 5-, and 8-story buildings were selected. Figure 1 shows the studied architectural plan of a building with three bays in each direction, 5 m each. The floor-to-floor height of this building is 3 m. All buildings considered in the present study had three bays in each direction of 5 m in length; the floor-to-floor height was 3.2 m.

Lateral resisting systems are the Special Moment Resisting Frames (SMRFs) in X and Y directions. The analyzed buildings are residential buildings in very high-risk zones on soil type III and are loaded and designed according to the Iranian national building code [37]. The soil in the Iranian national building code is classified according to Table 1.

The dead and live loads of all stories were presumed to amount to 6.5 kN/m^2 and 2.0 kN/m^2, respectively. For the roof of the building, the loads were equal to 4.5 kN/m^2 and 1.5 kN/m^2, respectively. The buildings with fixed bases were designed according to AISC 360-10 [38] in the ETABS software. The view

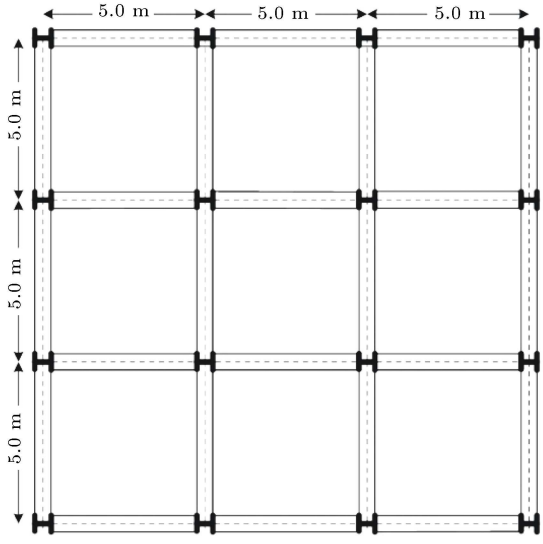

Figure 1. Schematic view of 3-, 5-, and 8-story buildings.

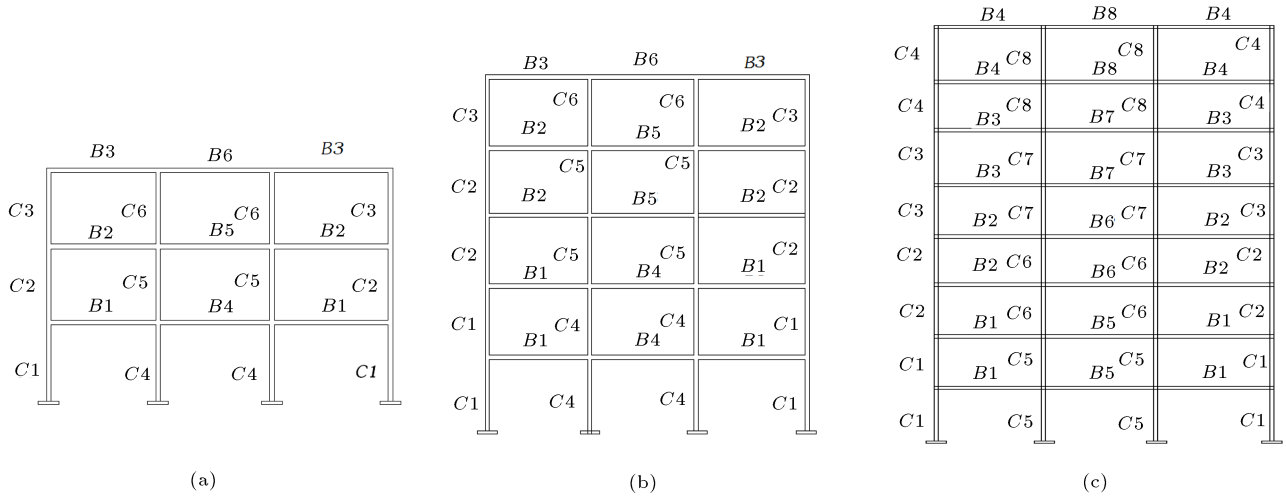

Figure 2. (a) The model of 3-story structure, (b) the model of 5-story structure, and (c) the model of 8-story structure (Figure 3). The finite element model of Soil-Structure Interaction (SSI) system in OpenSees.

Table 1. Soil classification in Iranian national building code [37].

Soil type	V_s (m/s)
I	$750 \leq V_s$
II	$375 \leq V_s \leq 750$
III	$175 \leq V_s \leq 375$
IV	$Vs \leq 175$

Table 2. The sections of the 3-story structure.

Column (length*width*thickness) (mm)	Beam	Section type
Tube 200 × 200 × 20	IPE* 300	$C1, B1$
Tube 200 × 200 × 20	IPE 300	$C2, B2$
Tube 200 × 200 × 20	IPE 270	$C3, B3$
Tube 280 × 280 × 20	IPE 400	$C4, B4$
Tube 280 × 280 × 20	IPE 300	$C5, B5$
Tube 280 × 280 × 20	IPE 270	$C6, B6$

*: European standard profiles.

of the structure type is shown in Figure 2 and member sections are listed in Tables 2–4.

2.2. Modeling of SSI

In the present study, the direct method was used for modeling SSI [39]. In this method, structure and soil are modeled simultaneously and their responses are determined by analyzing the SSI system in each time step. To this end, modeling and obtaining the nonlinear dynamic responses of the SSI system are performed using OpenSees, i.e., an open-source finite element software product [40]. The finite element model of the SSI system adopted in this study is shown in Figure 3.

Table 3. The sections of the 5-story structure.

Column (length*width*thickness) (mm)	Beam	Section type
Tube 240 × 240 × 20	IPE* 360	$C1, B1$
Tube 240 × 240 × 20	IPE 360	$C2, B2$
Tube 180 × 180 × 20	IPE 240	$C3, B3$
Tube 340 × 340 × 20	IPE 400	$C4, B4$
Tube 300 × 300 × 20	IPE 400	$C5, B5$
Tube 240 × 240 × 20	IPE 240	$C6, B6$

*: European standard profiles.

Table 4. The sections of the 8-story structure.

Column (length*width*thickness) (mm)	Beam	Section type
Tube 340 × 340 × 20	IPE*450	$C1, B1$
Tube 340 × 340 × 20	IPE 450	$C2, B2$
Tube 280 × 280 × 20	IPE 450	$C3, B3$
Tube 200 × 200 × 20	IPE 360	$C4, B4$
Tube 400 × 400 × 20	IPE 450	$C5, B5$
Tube 400 × 400 × 20	IPE 450	$C6, B6$
Tube 340 × 340 × 20	IPE 450	$C7, B7$
Tube 280 × 280 × 20	IPE 360	$C8, B8$

*: European standard profiles.

In the present study, the direct method was used to simulate SSI in which both structure and soils are modeled concurrently. In addition, in each time step, the responses are measured by assessing SSI system. Hence, the OpenSees software was used to obtain the nonlinear dynamic responses. Figure 3 illustrates the

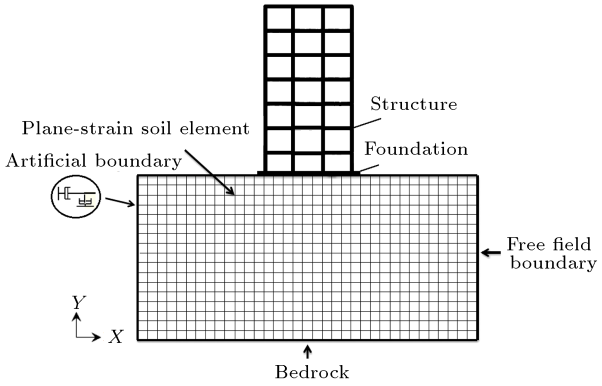

Figure 3. The finite element model of Soil-Structure Interaction (SSI) system in OpenSees.

finite element method of the SSI system adopted in the present study.

Previous studies have demonstrated that the distance from the structure center to the soil finite element model boundary varies by 2–3 times the foundation radius in the vertical direction and 3–4 times the foundation radius in the horizontal direction, in which the effect of the reflexive waves is negligible [16]. Therefore, in the present study, the soil domain with a total length of 100 m and a depth of 30 m was modeled using isoparametric four-node quadrilateral finite elements with two degrees of freedom per node.

The conditions of the soil domain are assumed as a plane strain with constant cross-plane thickness equal to the inter-frame distance. The modified pressure-independent multi-yield-surface J_2 plasticity model [41] (see Figure 4) was adopted as a constitutive model of the soil domain. Furthermore, some soil parameters depend on the shear wave velocity of soil, V_s. In this study, the parameter V_s for the soil type III is considered 300 m/s. The value of other parameters for the pressure-independent multi-yield plasticity model is selected according to the recommendation of the OpenSees manual.

In order to model radiation damping and prevent the reflection of outward propagating dilatational and shear waves back into the model, vertical and horizontal Lysmer-Kuhlemeyer [42] dashpots, as seen in Figure 3, are adopted in the free field boundary of the soil. The dashpots are modeled based on a zero-length element and the viscous uniaxial material. Of note, further details of the Lysmer-Kuhlemeyer dashpot are found in [42]. Furthermore, a raft foundation was considered rigid and the connection between the soil and the structure was obtained using common nodes and appropriate constraints. In order to ensure equal displacements for both the soil and the foundation of the structure, the constraints were applied by equal commands in X and Y directions.

Modeling the steel SMRF is considered using a lumped plasticity approach. In this approach, the beams and columns of the steel SMRF are modeled with elastic beam-column elements connected by zero-length elements which serve as rotational springs to represent the nonlinear behavior of the structure. The rotational springs at the member ends follow a bilinear hysteretic response based on the Ibarra-Medina-Krawinkler (IMK) model [43]. Figure 5 shows the properties of the IMK model. As shown in Figure 5, the five parameters expressed in [44] can be considered to deal with the nonlinearity of the model.

In the steel SMRF, the panel zone is deformed due to the shear force produced by the opposing moments in the beams and columns. To capture the deformation, this study utilizes the panel zone and explicitly models it by using the proposed approach [45]. Accordingly, a rectangular region is adopted that comprises eight very stiff elastic beam-column elements with one zero-length element that serves as a rotational spring to represent

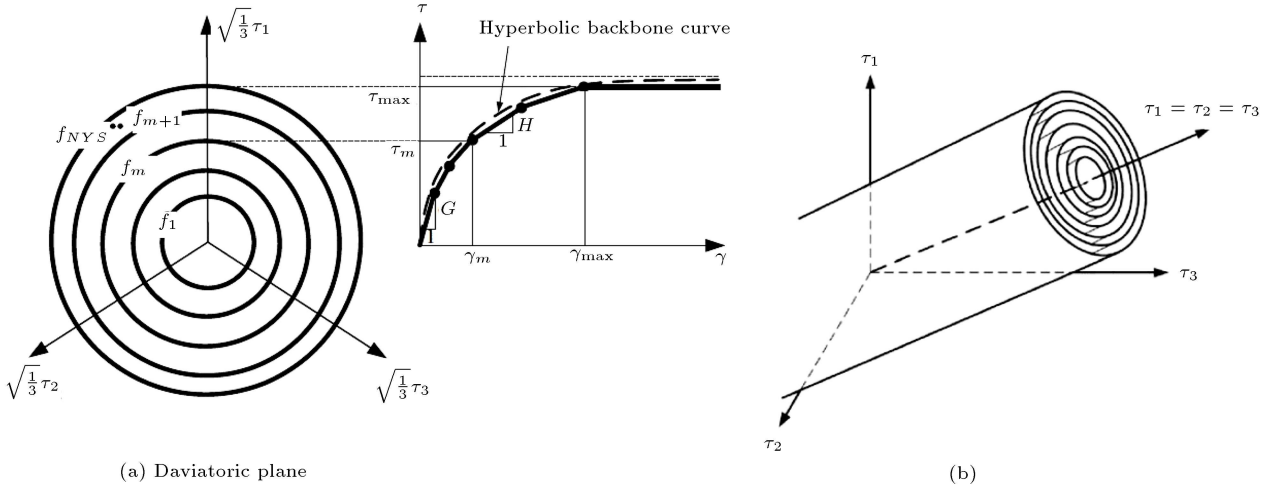

(a) Daviatoric plane (b)

Figure 4. Yield surfaces of multi-yield-surface J_2 plasticity model: (a) Octahedral shear stress-strain and (b) von Mises multi-yield surfaces [26].

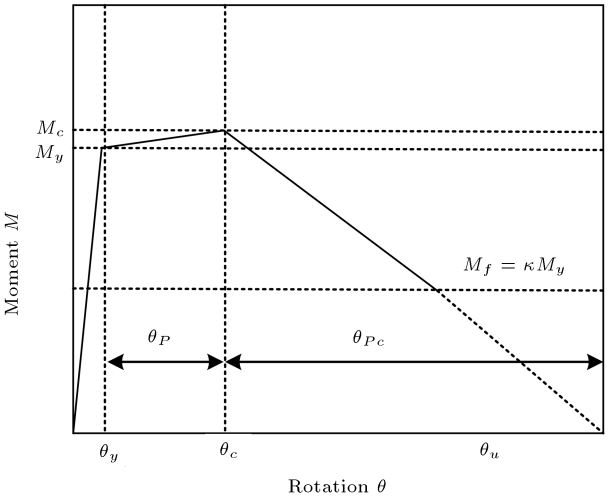

Figure 5. Monotonic moment-rotation relationship for the modified Ibarra-Median-Krawinkler (IMK) deterioration model [44].

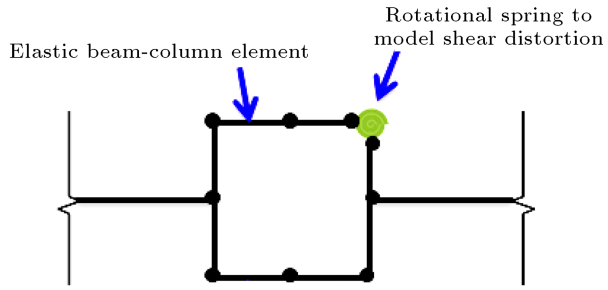

Figure 6. Schematic representation of a typical panel zone [40].

Table 5. The Soil-Structure Interaction (SSI) effects on the fundamental period of the designed frames.

Number of stories	Fundamental period (s)	
	Without SSI	With SSI
5	0.68	0.78
8	0.88	0.91
3	0.39	0.48

shear distortions in the panel zone (see Figure 6). At the three corners of the panel zone, except for the spring, the members are connected by a simple pin connection achieved by employing the equalDOF command in OpenSees. Hysteretic material was used to create a trilinear backbone behavior [45].

The damping matrix for the SSI system was assigned by assembling the corresponding damping matrices of the steel SMRF and soil. The damping matrix of the steel SMRF and soil was obtained based on Rayleigh's method [46]. To obtain these matrices, the damping ratios of the steel SMRF and soil were set to 2% and 10%, respectively. Furthermore, Table 5 shows the fundamental period of the designed frames with and without the SSI effects.

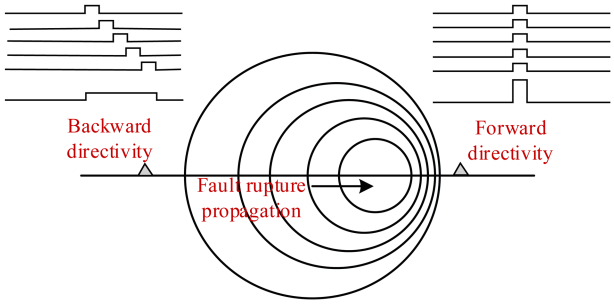

Figure 7. Forward, backward, and neutral directivity zones in a region close to an active fault [50].

3. Near-field earthquakes close to the fault under forward directivity effect

Besides the failure mechanism and type of faulting, the geometrical position and the place of a fault are other important criteria, particularly in the case of near-field earthquakes close to the fault. In near-fault earthquakes, the geometrical position of a fault and its corresponding place are of significance besides the failure mechanism and type of faulting. The response to ground velocity during an earthquake has a pulse-like shape with a long period of stimulation as a strike [47]. The amplitude of this pulse depends on the directivity of failure propagation to the site. Since the failure propagation velocity is nearly equal to the velocity of shear wave propagation, if the fault failure spreads to the considered place, the waves in a short-term period will reach the place and cause a high-amplitude and long-term pulse; thus, this phenomenon is called forward-effect directivity. If the failure occurs in the escape direction, the waves will reach there and, thus, it is defined as backward directivity, while the failure directivity which is neither close to the location nor far from it is called neutral directivity (see Figure 7) [48]. Pulse motion is stimulated through the permanent displacement of the ground due to surface failure. The pulses derived from surface failure are different from the ones caused by forward directivity [47].

The present paper focuses on the effect of pulse caused by forward directivity that causes the most extensive damage to the structure according to the obtained results of previous studies [23,49].

3.1. Selection of ground motions

To conduct a time history analysis of structures, choosing a suitable record is essential. Hence, in the present study, 14 real ground motion records were selected from the PEER-NGA database. The properties of these records are summarized in Tables 6 and 7. In order to analyze the nonlinear time history of the above records, a total of 7 earthquake records related to near-field earthquakes subjected to forward directivity and 7 records of far-field earthquakes were selected. The far-field ground motions for bedrock at a distance of

Table 6. The characteristics of far-field ground motions.

No.	Year	Earthquake	Station	Comp.	M_w	PGA (g)	PGV (m/s)	PGD (cm)	R (km)
1	2003	San Simeon_CA	Diablo Canyon Power Plant	H2	6.5	0.046	0.087	5.55	37.92
2	1999	Duzce_Turkey	Lamont 1060	E	7.1	0.053	0.057	5.28	25.78
3	2004	Niigata_Japan	FKSH07	NS	6.6	0.143	0.023	1.29	52.15
4	1999	Chi-Chi_Taiwan-06	HWA002	N	6.3	0.032	0.03	1.36	47.81
5	2008	Iwate_Japan	MYGH04	NS	6.9	0.22	0.054	3.24	40.42
6	1971	San Fernando	Pasadena	270	6.6	0.204	0.12	1.35	21.5
7	1994	Northridge-01	Vasquez	0	6.7	0.151	0.183	2.84	23.1

Table 7. The characteristics of near-field ground motions.

No.	Year	Earthquake	Station	Comp.	M_w	PGA (g)	PGV (m/s)	PGD (cm)	R (km)
1	1995	Kobe	Kobe University	90	6.9	0.311	30.88	0.074	0.9
2	1999	Kocaeli	Gebze	0	7.51	0.26	44.62	0.41	7.75
3	1992	Landers	Lucerne	345	7.28	0.788	56.21	1.021	2.19
4	1989	Loma Prieta	Los Gatos Dam	0	6.93	0.442	85.69	0.1733	3.22
5	1989	Loma Prieta	Gilroy Array #1	1090	6.93	0.484	32.48	0.156	8.84
6	1994	Northridge-01	Pacoima Dam (downstr)	PAC265	6.69	0.433	30.11	0.054	4.92
7	1971	San Fernando	Pacoima Dam (upper left abut)	254	6.61	1.238	57.27	0.128	0

20 to 60 km of non-pulse-like type were selected. The magnitude of these records ranged from 6.5 to 7.1. The magnitude of near-field earthquakes ranged from 6.61 to 7.51 and was recorded at a distance of 10 km from the fault. Of note, ground motion records shown in Tables 6 and 7 were selected based on $V_s \geq 750$ m/s (i.e., bedrock condition).

4. Evaluation of buildings seismic response

Generally, 42 non-linear time history analyses of the 14 mentioned records and buildings under study were carried out. Maximum acceleration was considered as the first criterion for the measurement of seismic demands in the overall level of system requirements. The value of maximum acceleration is shown in Figure 8 and it is obtained through the nonlinear time history analyses in two groups of earthquake records for buildings with a SMF system (3-, 5-, and 8-story) in both groups of earthquake records.

Evaluating the acceleration of the stories of all structures under the effect of near- and far-field earthquakes demonstrated that the maximum acceleration of the stories of the 3-story building was 18.39 m/s^2, which was obtained by applying record no. 7 to the structure. In the 5-story structure, this parameter was 25.35 m/s2 which occurred in the second story and subjected to record no. 3. Furthermore, the maximum acceleration of the 8-story structure was 26.17 m/s^2, which was also observed in the second story under the effect of record no. 7. On the other hand, the maximum acceleration values of 3-, 5-, and 8-story structures under the effect of far-field records were 8.95, 23.31, and 27.33 m/s^2, respectively, and were associated with records no.7, 6, and 5, respectively. Following a review of the current charts in Figure 8, it can be seen that as the stories leveled up under the effect of both groups of records, the maximum values of acceleration of stories increased. Table 8 reports the results of a comparison of the maximum average acceleration of stories under the effect of far- and near-field earthquakes.

The results of the present study illustrated that under the effect of near-field earthquakes, the maximum displacement of stories of the 3-story building was 80 mm, which occurred at the top story and under record no. 7. In the 5-story building, the maximum displacement of stories was recorded as 330 mm, where the second story experienced displacement subjected to record no. 4.

Table 8. Comparison of the maximum average acceleration of the stories under the effect of far- and near-field earthquakes.

Story	Near fault (m/s^2)	Far fault (m/s^2)	Near/far
3	11.12	5.47	2.03
5	19.39	15.95	1.22
8	20.02	14.25	1.41

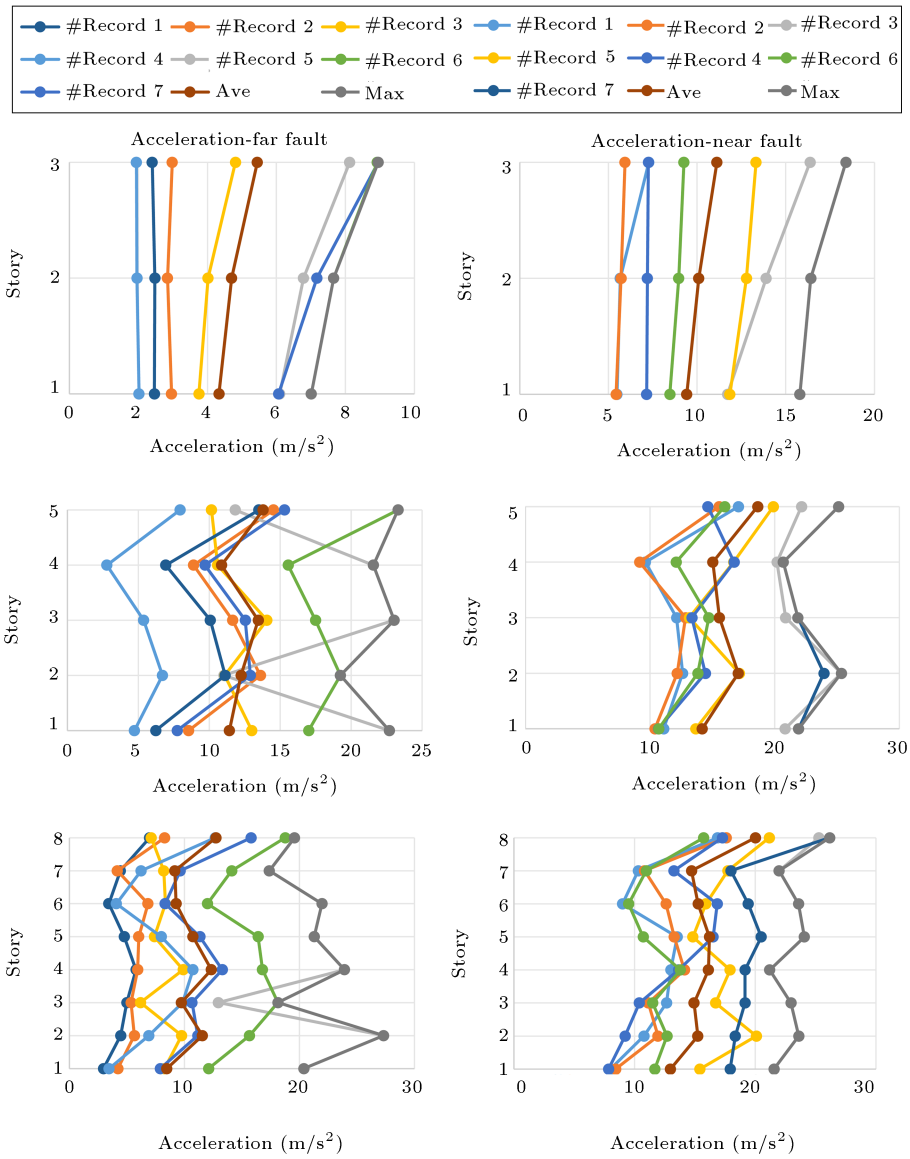

Figure 8. Maximum accelerations of 3-, 5-, and 8-story buildings subjected to far- and near-field earthquakes.

The maximum displacement of the 8-story structure occurred in the second story and under the influence of record no. 4, where the value of this displacement was 390 mm. On the other hand, the maximum displacement values of 22 mm, 121 mm, and 103 mm were obtained for 3-, 5-, and 8-story buildings and, in all of the three structures, record no. 6 showed these values. The results of comparing the average displacement values of stories under the effect of near- and far-field earthquakes are shown in Table 9. Figure 9 shows the maximum displacement of the stories of all of the three structures.

One of the important steps in seismic design is the estimation and control of structural deformation so as to increase the overall stability of the building during an earthquake. Restricting the inter-story drift of the structure, apart from the control of the overall structural stability, prevents damages to non-structural components including mechanical equipment and architectural elements. Furthermore, inter-story drift of the stories can be a measure of the calmness of the residents against displacements stemming from wind load and the amount of structural damage. The results demonstrate that the angle values of inter-story drift of the stories can be indicative of the performance

Table 9. Comparison of the average displacement under the effect of far- and near-field earthquakes.

Story	Near fault (mm)	Far fault (mm)	Near/Far
3	40	10	4
5	150	50	3
8	210	50	4.2

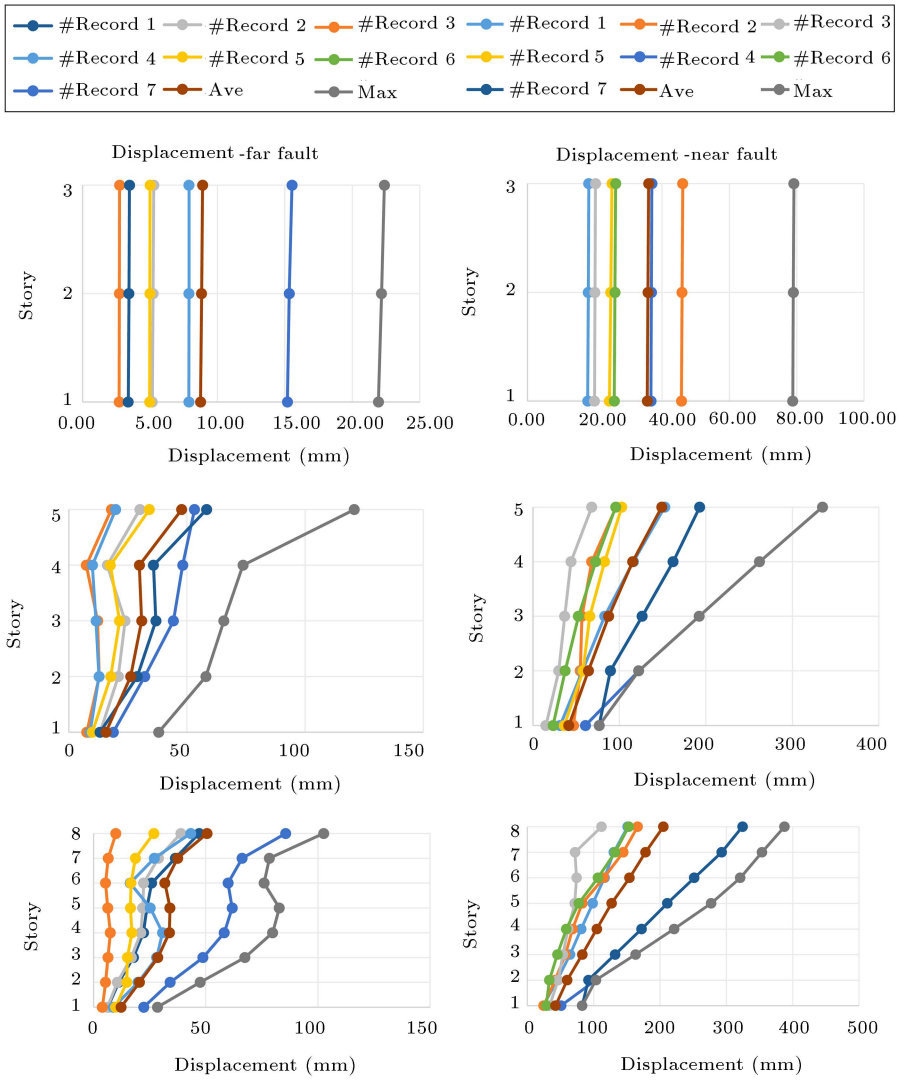

Figure 9. Maximum displacements of 3-, 5-, and 8-story buildings subjected to far- and near-field earthquakes.

of structural and non-structural components, such that if the angle of the inter-story drift ratio is 0.001, the damage to non-structural components will be probable and if the value of this parameter reaches 0.007, non-structural and structural damages will be definitive and probable, respectively. On the other hand, if the angle of the inter-story drift ratio exceeds 0.015, the non-structural and structural damages will definitely and probably occur, respectively [51]. Another reason for restricting the lateral deformation of the structure is the control of the $P-\Delta$ effects, especially in the near-fault field [51].

After evaluating the analysis results of nonlinear time histories, it was determined that in near-field earthquakes, the maximum inter-story drift ratio of the story in the 3-story building was 0.00; in the 5-story structure, the maximum drift ratio value was 0.024 in the fourth story and record no. 4 caused this displacement. Moreover, the maximum drift ratio value of the 8-story building was 0.0196 and occurred in the third story under the effect of record no. 4.

On the other hand, the maximum drift ratio values of 3-, 5-, and 8-story buildings under the effect of far-field earthquakes were 0.00007, 0.0205, and 0.0099, respectively, and record no. 6 caused this drift ratio value in all of the three structures. The graphs in Figure 10 show the drift ratio of the stories under the effect of near- and far-field earthquakes; for a more accurate investigation, the average drift ratio of the structures is reported in Table 10.

Based on a summary of the results reported in graphs of Figure 11 associated with the maximum velocity of stories under the effects of far- and near-field earthquakes, it can be concluded that in near-field earthquakes, the maximum velocity of every story of the 3-story building was 0.83 m/s.

This velocity was recorded at the third story and record no. 7 caused this velocity. In the 5-story build-

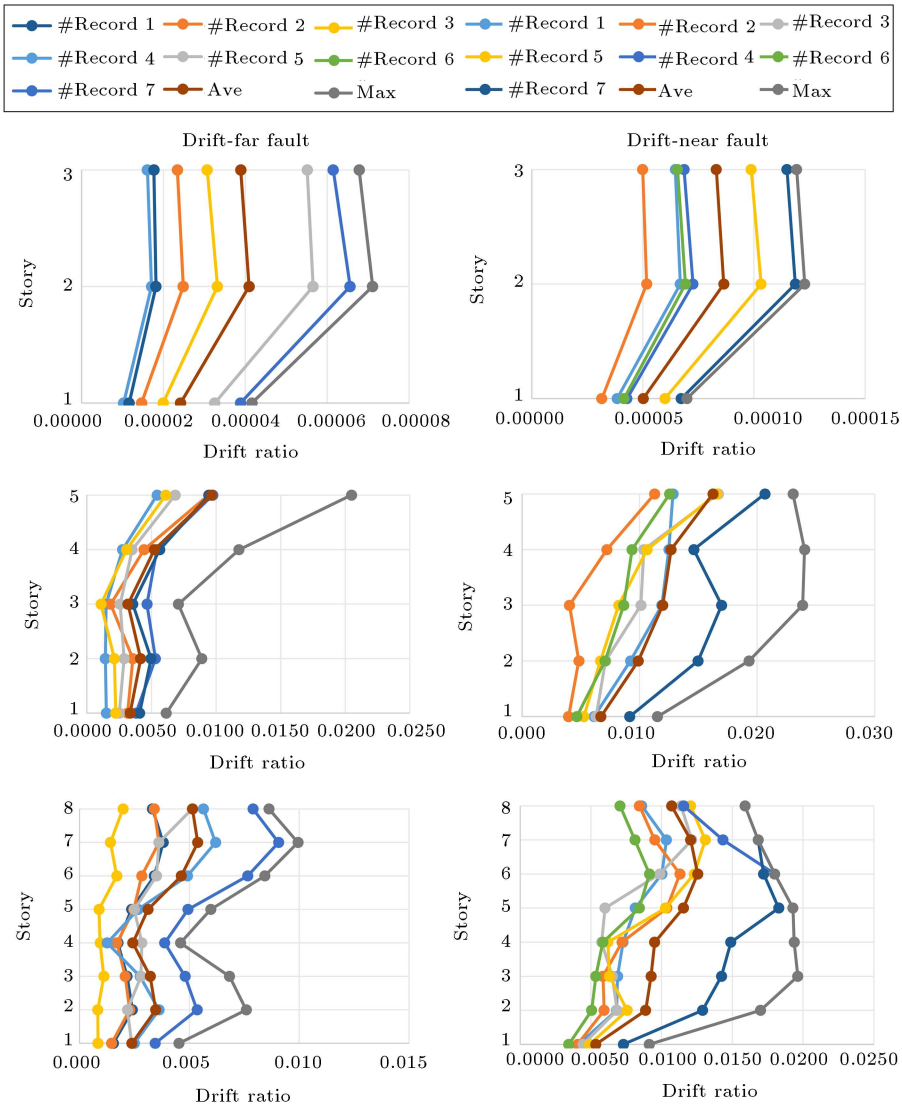

Figure 10. Maximum inter-story drift ratio of 3-, 5-, and 8-story buildings subjected to far- and near-field earthquakes.

Table 10. Comparison of the average inter-story drift ratio under the effect of the near- and far-field earthquakes.

Story	Near fault	Far fault	Near/far
3	0.00009	0.00004	2.25
5	0.02	0.01	2
8	0.0134	0.0057	2.35

Table 11. The comparison of the average velocity subjected to the far- and near-field earthquakes.

Story	Near fault (m/s)	Far fault (m/s)	Near/far
3	0.49	0.15	3.27
5	1.37	0.66	2.08
8	1.46	0.69	2.16

ing, the maximum velocity of the story was 2.03 m/s and occurred in the fifth story subjected to record no. 4. In this building, the eighth story experienced maximum velocity under the effect of record no. 4. The values of the effect of the far-field earthquakes in X, Y, Z directions were 0.326, 1.28, and 1.34, respectively, in which record no. 6 caused these displacements to occur.

Therefore, it can be concluded that the maximum velocity value of the stories increases by raising the stories in structures. A comparison of the average velocity under the effects of far- and near-field earthquakes is shown in Table 11.

By comparing the maximum values of the axial force created in stories under the effect of far- and near-field earthquakes, it becomes clear that, in near-field earthquakes, the maximum axial force generated in the 3-, 5- and 8-story buildings amounted to 5.96 kN, 12.63 kN, and 22.84 kN, respectively. In all of three

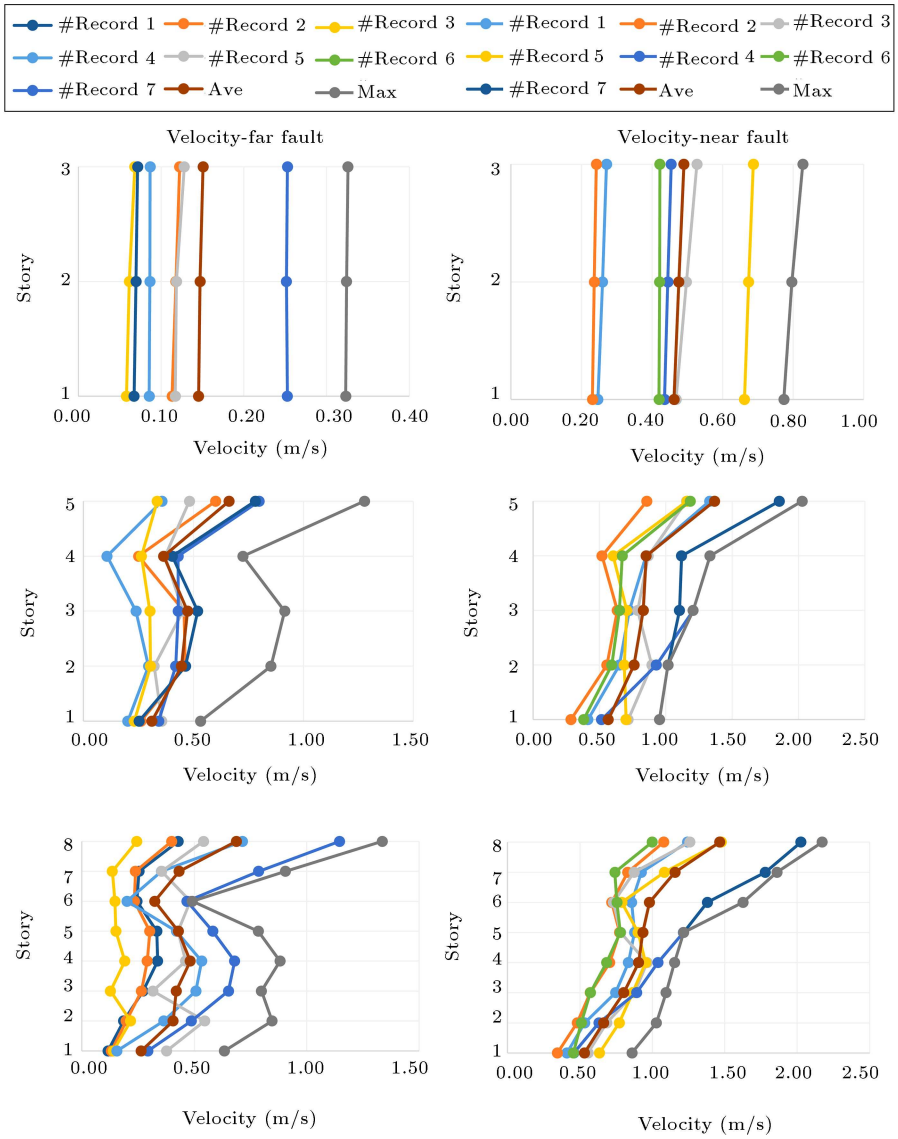

Figure 11. Maximum velocities of 3-, 5-, and 8-story buildings subjected to far- and near-field earthquakes.

buildings, record no. 7 produced these force values in columns. With similar investigations into the results of the structural analysis of the effect of far-field records, it can be concluded that the maximum axial force on the column in the 3-, 5-, and 8-story buildings is 3.87 kN, 10.90 kN, and 18.35 kN, respectively, and the application of record no. 6 caused the forces to appear. Tables 12 to 14 show the comparison of the maximum axial force values of columns in all of the three structures. Figure 12 shows the numbering of the columns of 3-, 5-, and 8-story structure. Figure 13 shows the maximum axial force on the columns of 3, 5, and 8-story buildings subjected to far- and near-field earthquakes. By comparing the maximum values of the moment in the stories under the effect of near- and far-field earthquakes, it is found that in the near field earthquakes, among all the 7 near-field earthquakes,

Table 12. The comparison of the maximum axial force generated in columns of the 3-story building under the effect of far- and near-field earthquakes.

No. of Story	No. of record	No. of column	Column axial force (kN)	Field type	Near/far
1	3	$C11$	5.96	Near	1.54
	6	$C11$	3.87	Far	
2	3	$C21$	3.32	Near	1.71
	6	$C21$	1.94	Far	
3	3	$C32$	1.44	Near	1.74
	7	$C33$	0.83	Far	

Table 13. The comparison of the maximum axial force generated in columns of the 5-story building under the effect of far- and near-field earthquakes.

No. of story	Field type	Column axial force (kN)	No. of column	No. of record	Near/far
1	Near	12.63	$C12$	7	1.16
	Far	10.90	$C13$	6	
2	Near	9.9	$C22$	7	1.21
	Far	7.59	$C23$	6	
3	Near	6.43	$C33$	7	1.22
	Far	5.29	$C33$	6	
4	Near	4.06	$C43$	3	1.06
	Far	3.82	$C43$	6	
5	Near	1.99	$C52$	7	0.96
	Far	2.07	$C53$	6	

Table 14. The comparison of the maximum axial force generated in columns of the 8-story building under the effect of far- and near-field earthquakes.

No. of story	Field type	Column axial force (kN)	No. of column	No. of record	Near/far
1	Near	22.84	$C12$	7	1.24
	Far	18.35	$C13$	6	
2	Near	18.48	$C22$	7	1.22
	Far	15.19	$C23$	6	
3	Near	15.07	$C32$	7	1.24
	Far	12.20	$C33$	6	
4	Near	12.24	$C42$	7	1.27
	Far	9.62	$C43$	6	
5	Near	9.67	$C52$	7	1.24
	Far	7.80	$C52$	6	
6	Near	6.56	$C62$	7	1.13
	Far	5.79	$C62$	6	
7	Near	3.86	$C71$	3	1.17
	Far	3.32	$C74$	6	
8	Near	1.93	$C82$	7	1.12
	Far	1.73	$C84$	5	

record no. 3 causes the maximum moment in the 3-story building and that the value of this moment is 10.85 kN.m. In the 5-story structure, the maximum moment is equal to 11.63 kN.m and occurs under the effect of record no. 4.

In the 8-story structure, following the application of record no. 4, the maximum produced moment in columns is 14.90 kN.m. The corresponding moment values of 3-, 5-, and 8-story structures subjected to far-field records are 6.64 kN.m, 7.34 kN.m, and 8.13 kN.m and record no. 6 caused the maximum moment to occur in all three structures. Tables 15 to 17 and Figure 14 show the maximum produced moment in columns of 3-, 5-, and 8-story buildings under the effect of far and near-field earthquakes.

In another comparison, the maximum values of the shear force of stories are shown in Figure 15

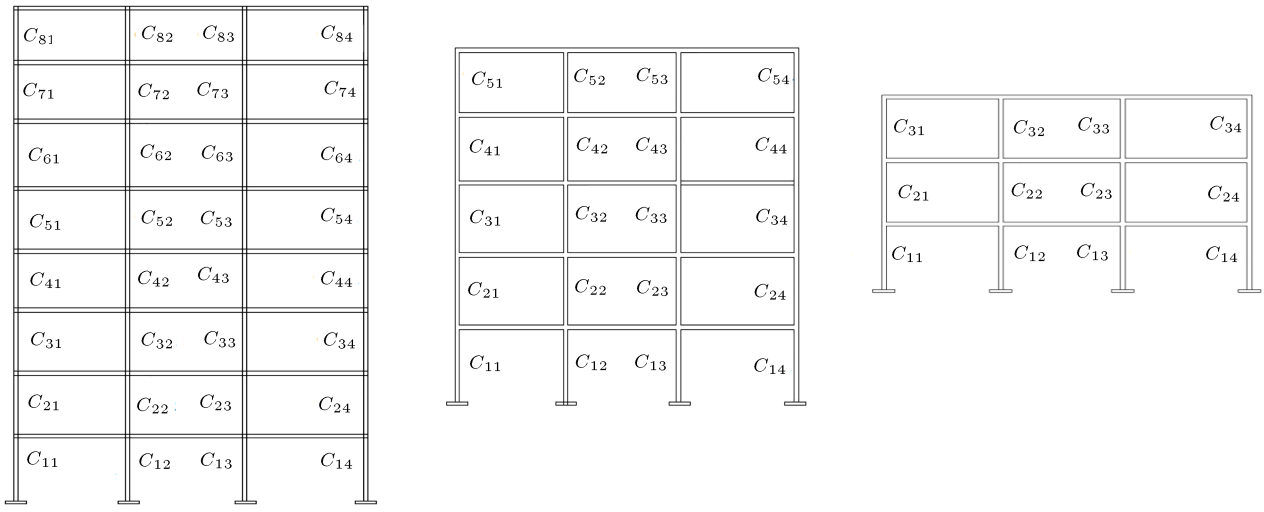

Figure 12. The numbering of the columns of 3-, 5-, and 8-story structures.

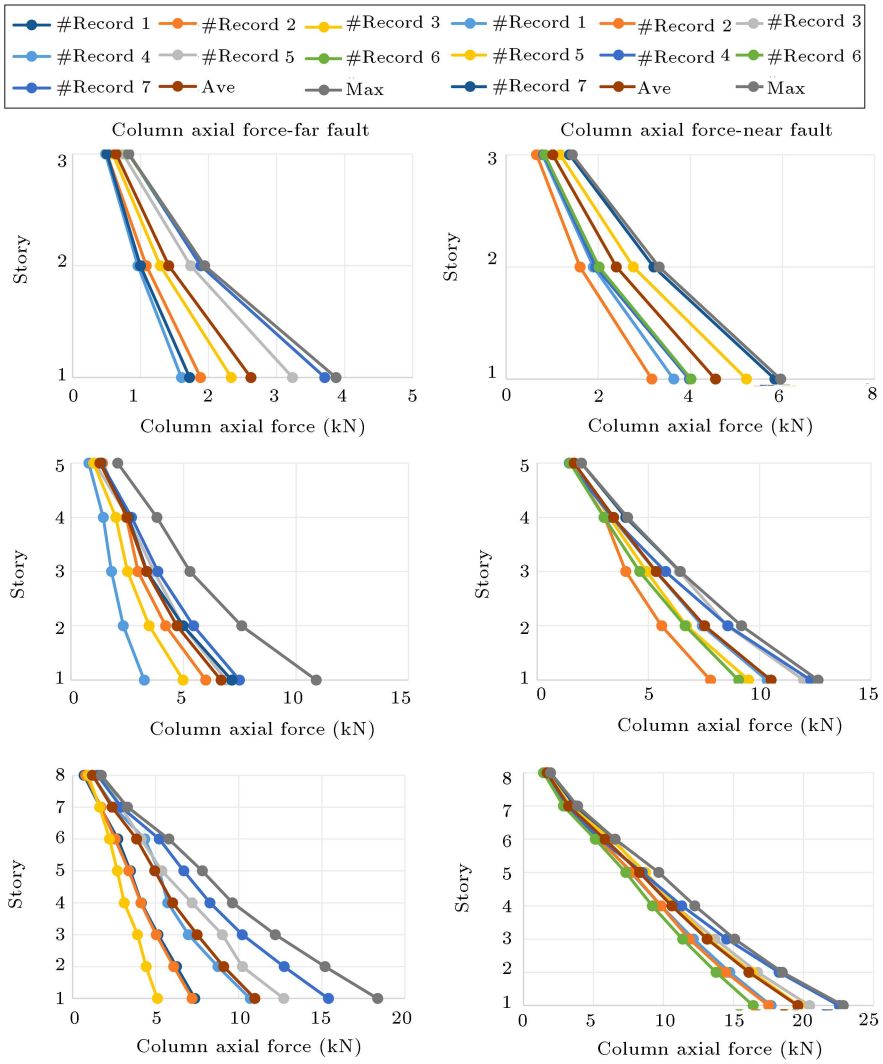

Figure 13. The maximum axial force created in columns of 3-, 5-, and 8-story buildings subjected to far- and near-field earthquakes.

Table 15. The comparison of the maximum moment produced in columns of the 3-story building subjected to far- and near-field earthquakes.

No. of story	Field type	Moment (kN.m)	No. of column	No. of record	Near/far
1	Near	10.85	$C11$	3	1.63
	Far	6.65	$C11$	6	
2	Near	3.77	$C21$	3	1.65
	Far	2.28	$C21$	7	
3	Near	2.69	$C33$	3	1.60
	Far	1.68	$C31$	6	

originating from the time history analysis of all three groups of structures under the effect of both groups of earthquake records. The results reported in Tables 18 to 20 indicate that the near-fault records do not

Table 16. The comparison of the maximum produced moment in columns of the 5-story building subjected to far- and near-field earthquakes.

No. of story	Field type	Moment (kN.m)	No. of column	No. of record	Near/far
1	Near	11.63	$C14$	4	1.58
	Far	7.34	$C13$	6	
2	Near	6.36	$C24$	4	1.59
	Far	3.99	$C23$	6	
3	Near	4.48	$C34$	4	1.42
	Far	3.15	$C32$	6	
4	Near	4.18	$C42$	7	1.08
	Far	3.87	$C43$	6	
5	Near	3.79	$C53$	3	0.96
	Far	3.93	$C53$	6	

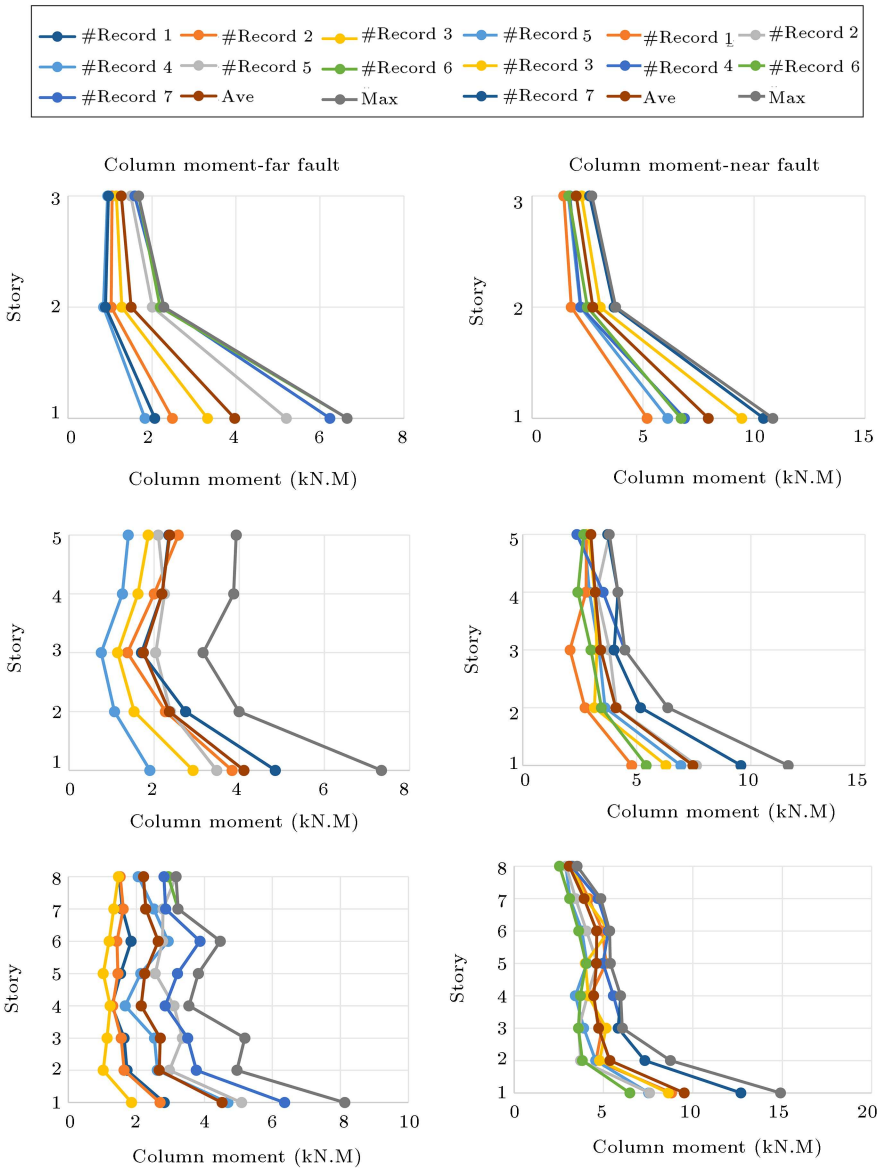

Figure 14. The maximum caused moment in columns of 3-, 5-, and 8-story buildings under the effect of the far- and near-field earthquakes.

necessarily produce higher shears than the far-fault records.

5. Conclusions

The present paper investigated the difference between the seismic behavior of the special steel moment frames under the effect of near-field earthquakes with forward directivity and that under far-field earthquakes. Using the holistic approach, soil-structure interaction and panel zone effects were considered in frame modeling. The direct method was used to model the soil-structure interaction. The results of the nonlinear time history analysis helped draw the following conclusions:

1. Compared to far-field earthquakes, near-field earthquakes caused a higher drift in all of the three structures. On average, the 3- and 5-story drift of buildings under the effect of near-field earthquakes was 2.25 and 2 times higher than that under far-field earthquakes. In addition, the average drift value of the 8-story building under the effect of near-field earthquakes was 2.35 times larger than that under far-field earthquakes.
2. The average displacement of the 3-story building under the effect of the near-field earthquake was 4 times larger than the far-field earthquake and it was respectively 3 and 4.2 times larger than that of 5- and 8-story buildings under earthquakes.
3. The maximum values of the axial force of column in the 3-, 5-, and 8-story buildings under the effect

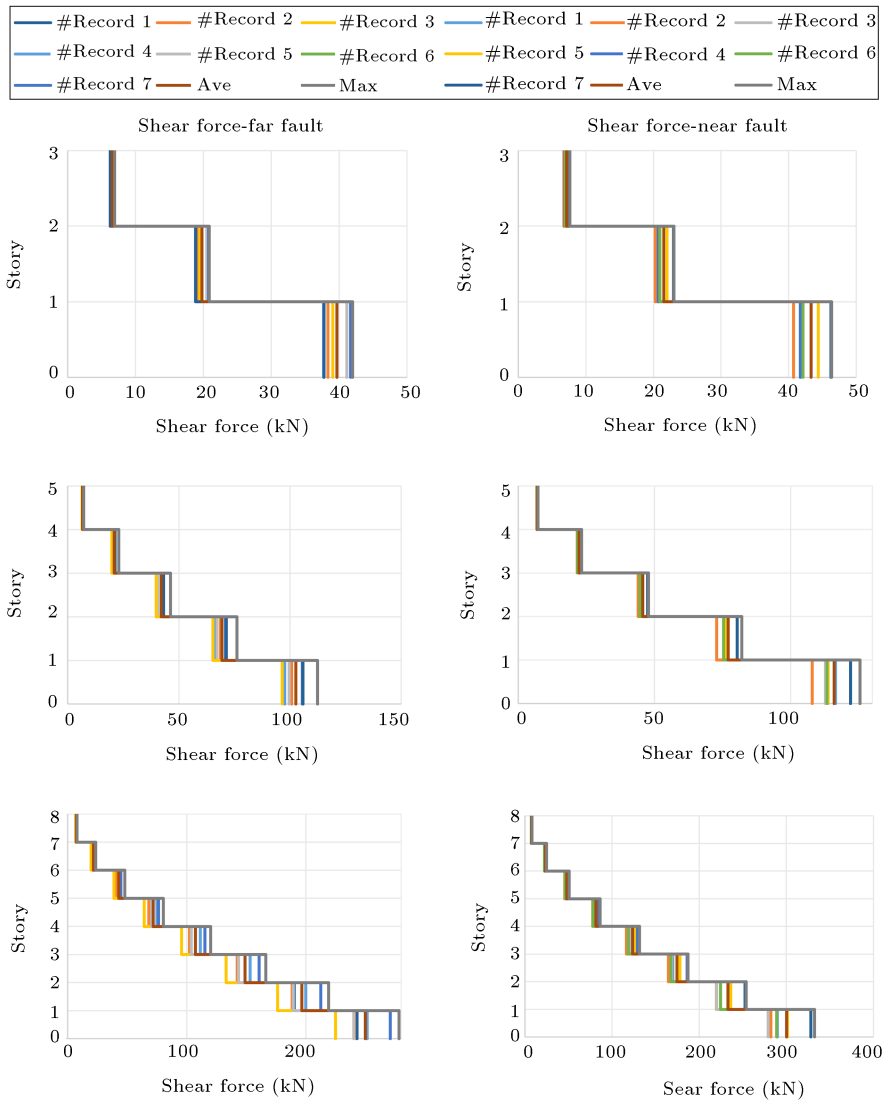

Figure 15. The maximum shear force generated in each story of 3-, 5-, and 8-story buildings under the effect of far- and near-field earthquakes.

of the near-field earthquake were 1.8, 1.58, and 1.79 times larger than those under the effect of the far-field earthquakes.

4. After investigating the average values of the moment in columns of buildings, it can be mentioned that in the 3-story building, the average value of the produced moment under the effect of near-field earthquakes was two times larger than that under the far-field earthquakes. Further, in 5- and 8-story buildings, the ratios of the average created moment are 1.81 and 2.18 times larger than those under far-field earthquakes.

5. The average base shear value of the 3-story building under the effect of near-field earthquakes was 1.09 times larger than that in the far-field earthquakes. In the 5- and 8-story buildings, this ratio increased to values that were 1.13 and 1.2 times larger than that under the far-field earthquake. By increasing the number of stories, the ratio value (the base shear under the effect of the far-field earthquake to the base shear under the effect of the near-field earthquake) increased.

6. The average acceleration under the effect of the near-field earthquake in the 3-story building was 2.03 times higher than that under the effect of the far-field earthquake. Further, in 5- and 8-story buildings, the average acceleration values subjected to near-field earthquakes were 1.22 and 1.41 times larger than those subjected to the far-field earthquakes.

7. The average produced velocity under the effect of the near-field earthquake in 3-, 5-, and 8-story buildings was 3.27, 2.08, and 2.16 times higher than those under the effect of far-field earthquakes.

Table 17. The comparison of the maximum produced moment in columns of the 8-story building subjected to far- and near-field earthquakes.

No. of story	Field type	Moment (kN.m)	No. of column	No. of record	Near/far
1	Near	14.90	$C13$	4	1.83
	Far	8.13	$C13$	6	
2	Near	8.74	$C23$	4	1.76
	Far	4.95	$C23$	6	
3	Near	6.06	$C33$	4	1.17
	Far	5.19	$C32$	6	
4	Near	5.96	$C42$	7	1.68
	Far	3.54	$C42$	6	
5	Near	5.38	$C52$	7	1.41
	Far	3.82	$C52$	6	
6	Near	5.35	$C63$	7	1.2
	Far	4.47	$C62$	6	
7	Near	4.85	$C73$	3	1.50
	Far	3.23	$C73$	6	
8	Near	3.53	$C82$	7	1.11
	Far	3.17	$C82$	6	

Table 18. The comparison of the maximum shear force generated in each story of the 3-story building under the effect of far- and near-field earthquakes.

No. of story	Field	Shear force (kN)	No. of record	Near/far
1	Near	46.3	3	1.10
	Far	42	6	
2	Near	23	3	1.10
	Far	20.9	6	
3	Near	76.1	3	1.10
	Far	69.2	6	

Table 19. The comparison of the maximum shear force generated in each story of the 5-story building under the effect of far- and near-field earthquakes.

No. of story	Field	Shear force (kN)	No. of record	Near/far
1	Near	125.5	4	1.11
	Far	112.3	6	
2	Near	82	4	1.08
	Far	76.1	6	
3	Near	47.8	4	1.03
	Far	46.2	6	
4	Near	23.2	7	1.01
	Far	22.9	6	
5	Near	72.1	7	1.00
	Far	71.9	6	

Table 20. The comparison of the maximum shear force generated in each story of the 8-story building under the effect of far- and near-field earthquakes.

No. of story	Field	Shear force (kN)	No. of record	Near/far
1	Near	332.4	4	1.19
	Far	278.3	6	
2	Near	253.9	4	1.16
	Far	219	6	
3	Near	187.2	7	1.13
	Far	166.4	6	
4	Near	131.6	7	1.10
	Far	119.9	6	
5	Near	862.5	7	1.07
	Far	802.6	6	
6	Near	509.6	7	1.08
	Far	470	6	
7	Near	248.9	7	1.06
	Far	234.7	6	
8	Near	820.1	7	1.06
	Far	773.3	6	

Acknowledgments

This work was supported by a 2016 Incheon National University Research Grant. The authors gratefully acknowledge these supports.

References

1. Shahbazi, S., Mansouri, I., Hu, J.W., and Karami, A. "Effect of soil classification on seismic behavior of SMFs considering soil-structure interaction and near-field earthquakes", *Shock and Vibration*, **2018**, pp. 1–17 (2018).
2. Farzampour, A. and Kamali Asl, A. "On seismic hazard analysis of the two vulnerable regions in Iran: deterministic and probabilistic approaches", *Proc. Conference*, New Zealand Society for Earthquake Engineering (NZSEE), Auckland, New Zealand (2014).
3. Farzampour, A. and Kamali-Asl, A. "Seismic hazard assessment for two cities in Eastern Iran", *Earthquake and Structures*, **8**(3), pp. 681–697 (2015).
4. Eser, M., Aydemir, C., and Ekiz, I. "Effects of soil structure interaction on strength reduction factors", *Proc., Procedia Engineering*, pp. 1696–1704 (2011).
5. Shakib, H. and Atefatdoost, G.R. "Effect of soil-structure interaction on torsional response of asymmetric wall type systems", *Proc., Procedia Engineering*, pp. 1729–1736 (2011).
6. Rodriguez, M.E. and Montes, R. "Seismic response and damage analysis of buildings supported on flexible soils", *Earthquake Engineering and Structural Dynamics*, **29**(5), pp. 647–665 (2000).
7. Behnamfar, F., Mirhosseini, S.M., and Alibabaei, H. "Seismic behavior of structures considering uplift and soil-structure interaction", *Advances in Structural Engineering*, **20**(11), pp. 1712–1726 (2017).
8. Shrestha, B., Hao, H., and Bi, K. "Seismic response analysis of multiple-frame bridges with unseating restrainers considering ground motion spatial variation and SSI", *Advances in Structural Engineering*, **18**(6), pp. 873–891 (2015).
9. Zheng, Y., Chen, B., and Chen, W. "Elasto-plastic seismic response of RC continuous bridge with foundation-pier dynamic interaction", *Advances in Structural Engineering*, **18**(6), pp. 817–836 (2015).
10. Fatahi, B. and Tabatabaiefar, S.H.R. "Effects of soil plasticity on seismic performance of mid-rise building frames resting on soft soils", *Advances in Structural Engineering*, **17**(10), pp. 1387–1402 (2014).
11. Hosseinzadeh, N. "Shake table study of Soil-Foundation-Structure Interaction (SFSI) effects in rocking and horizontal motions of the building structures", *Proc., 9th US National and 10th Canadian Conference on Earthquake Engineering 2010, Including Papers from the 4th International Tsunami Symposium* (2010).
12. Nateghi-A, F. and Rezaei-Tabrizi, A. "Nonlinear dynamic response of tall buildings considering structure-soil-structure effects", *Structural Design of Tall and Special Buildings*, **22**(14), pp. 1075–1082 (2013).
13. Liao, H.J., Liu, J., Zhao, V.G., and Xiao, Z.H. "Analysis of soil-structure interaction with finite element method", *Key Engineering Materials*, **340–341**, pp. 1279–1284 (2007).
14. Sáez, E., Lopez-Caballero, F., and Modaressi-Farahmand-Razavi, A. "Effect of the inelastic dynamic soil-structure interaction on the seismic vulnerability assessment", *Structural Safety*, **33**(1), pp. 51–63 (2011).
15. El Ganainy, H. and El Naggar, M.H. "Seismic performance of three-dimensional frame structures with underground stories", *Soil Dynamics and Earthquake Engineering*, **29**(9), pp. 1249–1261 (2009).
16. Tabatabaiefar, H.R. and Massumi, A. "A simplified method to determine seismic responses of reinforced concrete moment resisting building frames under influence of soil-structure interaction", *Soil Dynamics and Earthquake Engineering*, **30**(11), pp. 1259–1267 (2010).
17. Gharehbaghi, S., Salajegheh, E., and Khatibinia, M. "Evaluation of seismic energy demand of reinforced concrete moment resistant frames considering soil-structure interaction effects", *Proc., Civil-Comp Proceedings*.
18. Khatibinia, M., Javad Fadaee, M., Salajegheh, J., and Salajegheh, E. "Seismic reliability assessment of RC structures including soil-structure interaction using wavelet weighted least squares support vector machine", *Reliability Engineering and System Safety*, **110**, pp. 22–33 (2013).
19. Khatibinia, M., Salajegheh, E., Salajegheh, J., and Fadaee, M.J. "Reliability-based design optimization of reinforced concrete structures including soil-structure interaction using a discrete gravitational search algorithm and a proposed metamodel", *Engineering Optimization*, **45**(10), pp. 1147–1165 (2013).
20. Masaeli, H., Khoshnoudian, F., and Ziaei, R. "Rocking soil-structure systems subjected to near-fault pulses", *Journal of Earthquake Engineering*, **19**(3), pp. 461–479 (2015).
21. Mitropoulou, C.C., Kostopanagiotis, C., Kopanos, M., Ioakim, D., and Lagaros, N.D. "Influence of soil-structure interaction on fragility assessment of building structures", *Structures*, **6**, pp. 85–98 (2016).
22. Farzampour, A. and Kamali Asl, A. "Seismic hazard assessment for two cities in Eastern Iran", *Earthquakes and Structures*, **8**(3), pp. 681–697 (2015).
23. Kalkan, E. and Kunnath, S.K. "Effects of fling step and forward directivity on seismic response of buildings", *Earthquake Spectra*, **22**(2), pp. 367–390 (2006).

24. Liu, H., Hung, C., and Cao, J. "Relationship between Arias intensity and the responses of reinforced soil retaining walls subjected to near-field ground motions", *Soil Dynamics and Earthquake Engineering*, **111**, pp. 160–168 (2018).

25. Sayyadpour, H., Behnamfar, F., and El Naggar, M.H. "The near-field method: a modified equivalent linear method for dynamic soil-structure interaction analysis. Part II: verification and example application", *Bulletin of Earthquake Engineering*, **14**(8), pp. 2385–2404 (2016).

26. Abell, J.A., Orbović, N., McCallen, D.B., and Jeremic, B. "Earthquake soil-structure interaction of nuclear power plants, differences in response to 3-D, 3×1-D, and 1-D excitations", *Earthquake Engineering and Structural Dynamics*, **47**(6), pp. 1478–1495 (2018).

27. Lee, J.H. "Nonlinear soil-structure interaction analysis in poroelastic soil using mid-point integrated finite elements and perfectly matched discrete layers", *Soil Dynamics and Earthquake Engineering*, **108**, pp. 160–176 (2018).

28. Emami, A.R. and Halabian, A.M. "Damage index distributions in RC dual lateral load-resistant multi-story buildings considering SSI effects under bidirectional earthquakes", *Journal of Earthquake and Tsunami*, **12**(1), 1850004 (2018).

29. Khoshnoudian, F., Ziaei, R., Ayyobi, P., and Paytam, F. "Effects of nonlinear soil-structure interaction on the seismic response of structure-TMD systems subjected to near-field earthquakes", *Bulletin of Earthquake Engineering*, **15**(1), pp. 199–226 (2017).

30. Bybordiani, M. and Arıcı, Y. "Effectiveness of motion scaling procedures for the seismic assessment of concrete gravity dams for near field motions", *Structure and Infrastructure Engineering*, **14**(10), pp. 1–16 (2018).

31. Cheng, X., Jing, W., Chen, J., and Zhang, X. "Pounding dynamic responses of sliding base-isolated rectangular liquid-storage structure considering soil-structure interactions", *Shock and Vibration*, **2017**, 8594051 (2017).

32. Behnamfar, F. and Sayyadpour, H. "The near-field method: a modified equivalent linear method for dynamic soil-structure interaction analysis. Part I: Theory and methodology", *Bulletin of Earthquake Engineering*, **14**(8), pp. 2361–2384 (2016).

33. Johari, A., Javadi, A.A., and Najafi, H. "A genetic-based model to predict maximum lateral displacement of retaining wall in granular soil", *Scientia Iranica*, **23**(1), pp. 54–65 (2016).

34. Azizkandi, A.S., Baziar, M.H., Modarresi, M., Salehzadeh, H., and Rasouli, H. "Centrifuge modeling of pile-soil-pile interaction considering relative density and toe condition", *Scientia Iranica*, **21**(4), pp. 1330–1339 (2014).

35. Tajammolian, H., Khoshnoudian, F., and Bokaeian, V. "Seismic responses of asymmetric steel structures isolated with the TCFP subjected to mathematical near-fault pulse models", *Smart Structures and Systems*, **18**(5), pp. 931–953 (2016).

36. Yin, S., Li, Y., Sandberg, M., and Lam, K. "The effect of building spacing on near-field temporal evolution of triple building plumes", *Building and Environment*, **122**, pp. 35–49 (2017).

37. Standard-2800 "Iranian code of practice for seismic resistant design of buildings, 4th Ed.", Building and Housing Research Center, Tehran, Iran (in Persian) (2014).

38. "ANSI/AISC360-10: Specification for Structural Steel Buildings", American Institute of Steel Construction, Chicago-Illinois, American Institute of Steel Construction, Chicago-Illinois (2010).

39. Jaya, K.P. and Meher Prasad, A. "Embedded foundation in layered soil under dynamic excitations", *Soil Dynamics and Earthquake Engineering*, **22**(6), pp. 485–498 (2002).

40. Mazzoni, S., McKenna, F., Scott, M.H., and Fenves, G.L. "OpenSees", *Command Manual*, http://OpenSees.berkeley.edu/wiki/index.php/Command_Manual (2014).

41. Zhang, Y., Conte, J.P., Yang, Z., Elgamal, A., Bielak, J., and Acero, G. "Two-dimensional nonlinear earthquake response analysis of a bridge-foundation-ground system", *Earthquake Spectra*, **24**(2), pp. 343–386 (2008).

42. Lysmer, J. and Kuhlemeyer, R.L. "Finite dynamic model for infinite media", *Journal of the Engineering Mechanics Division*, **95**(4 EM), pp. 859–877 (1969).

43. Ibarra, L.F., Medina, R.A., and Krawinkler, H. "Hysteretic models that incorporate strength and stiffness deterioration", *Earthquake Engineering and Structural Dynamics*, **34**(12), pp. 1489–1511 (2005).

44. Lignos, D.G. and Krawinkler, H. "Deterioration modeling of steel components in support of collapse prediction of steel moment frames under earthquake loading", *Journal of Structural Engineering*, **137**(11), pp. 1291–1302 (2011).

45. Gupta, A. and Krawinkler, H. "Seismic demands for performance evaluation of steel moment resisting frame structures", Report no. 132., John A Blume Earthquake Engineering Center, Stanford University (1999).

46. Clough, R.W. and Penzien, J., *Dynamics of Structures*, McGraw-Hill Companies, New York (1975).

47. Decanini, L., Mollaioli, F., and Saragoni, R. "Energy and displacement demands imposed by near-source ground motions", *Proc., Proceedings of the 12th World Conference on Earthquake Engineering* (2000).

48. Singh, J.P. "Earthquake ground motions: Implications for designing structures and reconciling structural damage", *Earthquake Spectra*, **1**(2), pp. 239–270 (1985).

49. Alavi, B. and Krawinkler, H. "Behavior of moment-resisting frame structures subjected to near-fault ground motions", *Earthquake Engineering and Structural Dynamics*, **33**(6), pp. 687–706 (2004).

50. Chioccarelli, E. "Design earthquakes for PBEE in far-field and near-source conditions", Ph.D. Thesis, University of Naples Federico II (2010).

51. Naeim, F., *The Seismic Design Handbook*, Springer, 2nd Edn. (2001).

Biographies

Shahrokh Shahbazi has completed his BSc studies of Civil Engineering in Kerman Institute of Higher Education, Kerman, Iran (2011). He further followed his education in Structural Engineering and as an MSc student, graduated from Free Institute of Higher Education of A.B.A, Ghazvin, Iran (2014). Ever since, he has focused on research fields of his interest including the interaction between soil and structure, near-field earthquake, concrete additives, and development of fragility curve. He currently serves as a supervisor engineer in TAT Investment Company.

Mohsen Khatibinia is an Associate Professor at the Civil Engineering Department at University of Birjand in Birjand, Iran. He received his PhD degree from Shahid Bahonar University of Kerman in 2013. He specializes in the areas of soil-structure interaction and structural optimization.

Iman Mansouri received his PhD degree from Department of Civil Engineering in Shahid Bahonar University of Kerman. Currently, he has been an Assistant Professor at Department of Civil Engineering, Birjand University of Technology. His research interests are in the area of nonlinear structural analysis, earthquake engineering, seismic retrofitting, performance-based design, and soft computing methods.

Jong Wan Hu received his PhD degree from School of Civil and Environmental Engineering, Georgia Institute of Technology, USA. He also worked as an Associate Research Fellow at the Korea Institute of S&T Evaluation and Planning (KISTEP) and an Assistant Administrator at the National S&T Council (NSTC) for two years. He is currently an Associate Professor in the Incheon National University. He has been active in the member of ASME and ASCE. His research interests are in the area of computational solid mechanics, smart materials, and plasticity modeling.